The 8th Asian Computational Fluid Dynamics Conference
Hong Kong, 10-14 January, 2010

Null-field boundary integral equation approach for hydrodynamic scattering by multiple circular and elliptical cylinders

***J. W. Lee* [1], *J. T. Chen* [2]**

1. *Department of Harbor and River Engineering, National Taiwan Ocean University, 2 Pei-Ning Road, Keelung, 202-24,Taiwan. E-mail: M98520012@mail.ntou.edu.tw*

2. *Department of Harbor and River Engineering, National Taiwan Ocean University, 2 Pei-Ning Road, Keelung, 202-24,Taiwan. E-mail: jtchen@mail.ntou.edu.tw*

Corresponding author ***J. T. Chen***

Abstract

In this paper, the null-field boundary integral formulation in conjunction with the degenerate kernel and the Mathieu function in the elliptic coordinates is proposed to solve the hydrodynamic scattering problem by multiple circular and elliptical cylinders. Based on the adaptive observer system, the present method can solve the water wave problem containing circular and elliptical cylinders at the same time in a semi-analytical manner. The closed-form fundamental solution is expressed in terms of the degenerate kernel in the polar and elliptic coordinates for circular and elliptical cylinders, respectively. Several examples are demonstrated to see the validity of the semi-analytical approach.

Keyword: *null-field boundary integral equation, degenerate kernel, Mathieu function, hydrodynamic scattering, elliptical cylinders.*

1. Introduction

The hydrodynamic scattering problems containing vertical cylinders subject to the incident plane wave become more interesting and important in the recent years. Based on the linearized wave theory for the constant depth of water depth, the study can be simplified to the two-dimensional Helmholtz problem. The exact solution of horizontal wave force on a single vertical circular cylinder was found by MacCamy and Fuchs [1]. For a single elliptical cylinder, the analytical solution of wave forces was derived by Goda and Yoshimi [2]. They used the method of separation variables to obtain the solutions in terms of the Mathieu and modified Mathieu functions. Au and Brebbia [3] used the boundary element method to revisit the water wave problem with a circular or an elliptical cylinder and made agreement with the analytical solutions [1, 2].

The previous works [1, 2] focused on circular and elliptical vertical cylinder. Regarding the problem with multiple circular cylinders, Spring and Monkmeyer. [4] applied the method of multiple scattering (or so-called addition theorem for the Bessel function) to obtain a solution for two circular cylinders. Not only identical radius but also unequal cases were considered. Similarly, Linton and Evan [5] also employed the method of multiple scattering to deal with the problem with arrays of vertical circular cylinders. Chatjigeorgiou and Mavrakos [6] extended the method of multiple scattering to solve the hydrodynamic diffraction with two parallel identical elliptical cylinders by using the addition theorem for the Mathieu functions which was proposed by Særmark [7]. This idea is similar to the multipole Trefftz method by Chen's group [8, 9], since the multipole concept and addition theorem are both used.

Recently, Chen *et al*. [10] applied the null-field boundary integral equation method (BIEM) in conjunction with the degenerate kernel and the Fourier series to solve the interaction of water wave problem containing multiple circular cylinders. The advantage of free of calculating principal values is gained. This approach is one kind of semi-analytical methods since errors only occur from the truncation of the number of the Fourier terms. Besides, it belongs to a meshless method since only collocation points on the boundaries are required, respectively.

However, Chen *et al*. [10] only dealt with the problem with circular cylinders. Accordingly, we aim to extend the null-field BIEM to solve the problem with elliptical cylinders in this paper. The closed-form fundamental solution is expanded to the degenerate kernel by using the elliptic coordinates [11]. Also, the unknown boundary densities are expanded by using the eigenfunction expansion. The advantage of free of calculating principal value is also reserved. Owing the complexity of addition theorem by expressing in different coordinates (polar to elliptic), the method of multiple scattering [4-6] may have difficulty to solve the water wave problem containing circular and elliptical cylinders. To avoid this difficulty, an adaptive observer system is proposed to solve the water wave problem containing both circular and elliptical cylinders at the same time in a semi-analytical manner

To demonstrate the validity of the present approach, three illustrative examples are given. One is a single elliptical cylinder that the analytical solution can be obtained by using the present approach. Another is two parallel identical elliptical cylinders. The other is the case containing one circular and one elliptical cylinder together. After comparing with the results of Au and Brebbia [3], Chatjigeorgiou and Mavrakos [6] and the BEM, agreement is made.

2. Problem statement and the present approach

2.1 Problem statement

The typical water wave problem is governed by the Laplace equation

$$\nabla^2 \Phi_T(\mathbf{x}, z; t) = 0, (\mathbf{x}, z) \in D, \tag{1}$$

where ∇^2 is the Laplacian operator, $\Phi_T(\mathbf{x}, z; t)$ is the total velocity potential, $\mathbf{x} = (x, y)$ and D is the domain of interest. According to the linearized wave theory and the method of separation variables, the total velocity potential can be written as

$$\Phi_T(\mathbf{x}, z; t) = u_T(\mathbf{x}) f(z) e^{-i\omega t}, \tag{2}$$

where

$$u_T(\mathbf{x}) = u_I(\mathbf{x}) + u_R(\mathbf{x}), \tag{3}$$

in which the subscripts I and R denote the incident wave and radiative potential, respectively, and

$$f(z) = \frac{-igA}{\omega} \frac{\cosh\left(k(z+h)\right)}{\cosh(kh)}, \tag{4}$$

where i is the imaginary number with $i^2 = -1$, g is the gravity constant, A is the amplitude of incident wave, ω is the angular frequency, k is the wave number and h is the water depth. By substituting the Eq. (2) into Eq. (1) and using Eq. (4), we have

$$(\nabla^2 + k^2) u_T(\mathbf{x}) = 0, \quad \mathbf{x} \in D, \tag{5}$$

where the incident wave potential is expressed by

$$u_I(\mathbf{x}) = e^{ik\left(x\cos(\alpha) + y\sin(\alpha)\right)}, \tag{6}$$

where α is the incident angle. Since the cylinder are assumed to be rigid, impermeable and stationary, the boundary condition is the Neumann type as shown below:

$$\frac{\partial u_T(\mathbf{x})}{\partial n_{\mathbf{x}}} = t_T(\mathbf{x}) = 0, \mathbf{x} \in B, \tag{7}$$

where $n_{\mathbf{x}}$ denotes the unit outward normal vector at the field point and B is the boundary on the cylinder surface.

2.2 Dual boundary integral formulations — the conventional version

Based on the Green's third identity, the dual boundary integral equations for the domain point are shown below:

$$2\pi u_R(\mathbf{x}) = \int_B T(\mathbf{s}, \mathbf{x}) u_R(\mathbf{s}) dB(\mathbf{s}) - \int_B U(\mathbf{s}, \mathbf{x}) t_R(\mathbf{s}) dB(\mathbf{s}), \quad \mathbf{x} \in D, \tag{8}$$

$$2\pi t_R(\mathbf{x}) = \int_B M(\mathbf{s}, \mathbf{x}) u_R(\mathbf{s}) dB(\mathbf{s}) - \int_B L(\mathbf{s}, \mathbf{x}) t_R(\mathbf{s}) dB(\mathbf{s}), \quad \mathbf{x} \in D, \tag{9}$$

where $\mathbf{s}$ is the source point, and $U(\mathbf{s}, \mathbf{x})$ is the fundamental function which satisfies

$$(\nabla^2 + k^2) U(\mathbf{s}, \mathbf{x}) = 2\pi\delta(\mathbf{x} - \mathbf{s}), \tag{10}$$

where δ is the Dirac-delta function. The other kernel functions $T(\mathbf{s}, \mathbf{x})$, $L(\mathbf{s}, \mathbf{x})$ and $M(\mathbf{s}, \mathbf{x})$ are defined by

$$T(\mathbf{s},\mathbf{x})=\frac{\partial U(\mathbf{s},\mathbf{x})}{\partial n_{\mathbf{s}}}, \tag{11}$$

$$L(\mathbf{s},\mathbf{x})=\frac{\partial U(\mathbf{s},\mathbf{x})}{\partial n_{\mathbf{x}}}, \tag{12}$$

$$M(\mathbf{s},\mathbf{x})=\frac{\partial^2 U(\mathbf{s},\mathbf{x})}{\partial n_{\mathbf{s}}\partial n_{\mathbf{x}}}, \tag{13}$$

where $n_{\mathbf{s}}$ denotes the unit outward normal vector at the source point. By moving the field point $\mathbf{x}$ to the boundary, the dual boundary integral equations for the boundary point can be obtained as follows:

$$\pi u_R(\mathbf{x})=C.P.V\int_B T(\mathbf{s},\mathbf{x})u_R(\mathbf{s})dB(\mathbf{s})-R.P.V\int_B U(\mathbf{s},\mathbf{x})t_R(\mathbf{s})dB(\mathbf{s}),\quad \mathbf{x}\in B, \tag{14}$$

$$\pi t_R(\mathbf{x})=H.P.V\int_B M(\mathbf{s},\mathbf{x})u_R(\mathbf{s})dB(\mathbf{s})-C.P.V\int_B L(\mathbf{s},\mathbf{x})t_R(\mathbf{s})dB(\mathbf{s}),\quad \mathbf{x}\in B, \tag{15}$$

where R.P.V., C.P.V. and H.P.V. denote the Riemann principal value (Riemann sum), Cauchy principal value and Hadamard (or so-called Mangler) principal value, respectively. By collocating the field point $\mathbf{x}$ on the complementary domain, we obtain the dual null-field boundary integral equations as shown below:

$$0=\int_B T(\mathbf{s},\mathbf{x})u_R(\mathbf{s})dB(\mathbf{s})-\int_B U(\mathbf{s},\mathbf{x})t_R(\mathbf{s})dB(\mathbf{s}),\quad \mathbf{x}\in D^c, \tag{16}$$

$$0=\int_B M(\mathbf{s},\mathbf{x})u_R(\mathbf{s})dB(\mathbf{s})-\int_B L(\mathbf{s},\mathbf{x})t_R(\mathbf{s})dB(\mathbf{s}),\quad \mathbf{x}\in D^c, \tag{17}$$

where D^c denote the complementary domain.

2.3 Dual null-field boundary integral formulations — the present version

By introducing the degenerate kernels, the collocation point in Eqs. (8), (9), (16) and (17) can be located on the real boundary free of calculating principal value. Therefore, the boundary integral equations can be rewritten in two parts as given in the following formulation of Eqs. (18) and (20), instead of three parts using Eqs. (8), (14) and (16) in the conventional BEM,

$$2\pi u_R(\mathbf{x})=\int_B T(\mathbf{s},\mathbf{x})u_R(\mathbf{s})dB(\mathbf{s})-\int_B U(\mathbf{s},\mathbf{x})t_R(\mathbf{s})dB(\mathbf{s}),\quad \mathbf{x}\in D\cup B, \tag{18}$$

$$2\pi t_R(\mathbf{x})=\int_B M(\mathbf{s},\mathbf{x})u_R(\mathbf{s})dB(\mathbf{s})-\int_B L(\mathbf{s},\mathbf{x})t_R(\mathbf{s})dB(\mathbf{s}),\quad \mathbf{x}\in D\cup B, \tag{19}$$

and

$$0=\int_B T(\mathbf{s},\mathbf{x})u_R(\mathbf{s})dB(\mathbf{s})-\int_B U(\mathbf{s},\mathbf{x})t_R(\mathbf{s})dB(\mathbf{s}),\quad \mathbf{x}\in D^c\cup B, \tag{20}$$

$$0=\int_B M(\mathbf{s},\mathbf{x})u_R(\mathbf{s})dB(\mathbf{s})-\int_B L(\mathbf{s},\mathbf{x})t_R(\mathbf{s})dB(\mathbf{s}),\quad \mathbf{x}\in D^c\cup B. \tag{21}$$

It is found that Eqs. (18)-(21) can contain the boundary point ($\mathbf{x}$ on B) since the kernel functions are expressed in terms of the degenerate kernel.

2.4 Expansions of fundamental solution, boundary density and incident plane wave using the polar and the elliptic coordinates

The closed-form fundamental solution as previously mentioned is

$$U(\mathbf{s},\mathbf{x})=-\frac{i\pi H_0^{(1)}(kr)}{2}, \tag{22}$$

where $r\equiv|\mathbf{x}-\mathbf{s}|$ is the distance between the field point and the source point and $H_0^{(1)}$ is the zeroth-order Hankel function of the first kind. To fully utilize the properties of circular and elliptic geometries, respectively, the degenerate (separable or finite-rank) kernel and the Fourier series or eigenfunction expansion are utilized for the analytical integration of boundary contour integrals. In the polar and elliptic coordinates, the field point $\mathbf{x}$ is expressed as $\mathbf{x}=(\rho_{\mathbf{x}},\phi_{\mathbf{x}})$ and $\mathbf{x}=(\xi_{\mathbf{x}},\eta_{\mathbf{x}})$, respectively, while the source point $\mathbf{s}$ is expressed as $\mathbf{s}=(\rho_{\mathbf{s}},\phi_{\mathbf{s}})$ and $\mathbf{s}=(\xi_{\mathbf{s}},\eta_{\mathbf{s}})$, respectively. By employing the addition theorem [11] for separating the source point and field point in the kernel functions, $U(\mathbf{s},\mathbf{x})$, $T(\mathbf{s},\mathbf{x})$, $L(\mathbf{s},\mathbf{x})$ and $M(\mathbf{s},\mathbf{x})$ are expanded in terms of degenerate kernel in the polar (Eqs. (23)-(26)) [10, 11] and the elliptic coordinates (Eqs. (28)-(31)) [11] as shown below:

$$U(\mathbf{s},\mathbf{x})=\begin{cases}\dfrac{-\pi i}{2}\displaystyle\sum_{m=0}^{\infty}\varepsilon_m J_m(k\rho_{\mathrm{s}})H_m^{(1)}(k\rho_{\mathrm{x}})\cos(m(\phi_{\mathrm{s}}-\phi_{\mathrm{x}})),\ \rho_{\mathrm{x}}\ge\rho_{\mathrm{s}},\\ \dfrac{-\pi i}{2}\displaystyle\sum_{m=0}^{\infty}\varepsilon_m J_m(k\rho_{\mathrm{x}})H_m^{(1)}(k\rho_{\mathrm{s}})\cos(m(\phi_{\mathrm{s}}-\phi_{\mathrm{x}})),\ \rho_{\mathrm{x}}<\rho_{\mathrm{s}},\end{cases}\tag{23}$$

$$T(\mathbf{s},\mathbf{x})=\begin{cases}\dfrac{-\pi k i}{2}\displaystyle\sum_{m=0}^{\infty}\varepsilon_m J_m'(k\rho_{\mathrm{s}})H_m^{(1)}(k\rho_{\mathrm{x}})\cos(m(\phi_{\mathrm{s}}-\phi_{\mathrm{x}})),\ \rho_{\mathrm{x}}>\rho_{\mathrm{s}},\\ \dfrac{-\pi k i}{2}\displaystyle\sum_{m=0}^{\infty}\varepsilon_m J_m(k\rho_{\mathrm{x}})H_m'^{(1)}(k\rho_{\mathrm{s}})\cos(m(\phi_{\mathrm{s}}-\phi_{\mathrm{x}})),\ \rho_{\mathrm{x}}<\rho_{\mathrm{s}},\end{cases}\tag{24}$$

$$L(\mathbf{s},\mathbf{x})=\begin{cases}\dfrac{-\pi k i}{2}\displaystyle\sum_{m=0}^{\infty}\varepsilon_m J_m(k\rho_{\mathrm{s}})H_m'^{(1)}(k\rho_{\mathrm{x}})\cos(m(\phi_{\mathrm{s}}-\phi_{\mathrm{x}})),\ \rho_{\mathrm{x}}>\rho_{\mathrm{s}},\\ \dfrac{-\pi k i}{2}\displaystyle\sum_{m=0}^{\infty}\varepsilon_m J_m'(k\rho_{\mathrm{x}})H_m^{(1)}(k\rho_{\mathrm{s}})\cos(m(\phi_{\mathrm{s}}-\phi_{\mathrm{x}})),\ \rho_{\mathrm{x}}<\rho_{\mathrm{s}},\end{cases}\tag{25}$$

$$M(\mathbf{s},\mathbf{x})=\begin{cases}\dfrac{-\pi k^2 i}{2}\displaystyle\sum_{m=0}^{\infty}\varepsilon_m J_m'(k\rho_{\mathrm{s}})H_m'^{(1)}(k\rho_{\mathrm{x}})\cos(m(\phi_{\mathrm{s}}-\phi_{\mathrm{x}})),\ \rho_{\mathrm{x}}\ge\rho_{\mathrm{s}},\\ \dfrac{-\pi k^2 i}{2}\displaystyle\sum_{m=0}^{\infty}\varepsilon_m J_m'(k\rho_{\mathrm{x}})H_m'^{(1)}(k\rho_{\mathrm{s}})\cos(m(\phi_{\mathrm{s}}-\phi_{\mathrm{x}})),\ \rho_{\mathrm{x}}<\rho_{\mathrm{s}},\end{cases}\tag{26}$$

where J_m is the m^{th} order Bessel function of the first kind and ε_m is the Neumann factor

$$\varepsilon_m=\begin{cases}1, & m=0,\\ 2, & m=1,2,\ldots,\infty,\end{cases}\tag{27}$$

and

$$U(\mathbf{s},\mathbf{x})=\begin{cases}-2\pi i\left(\displaystyle\sum_{m=0}^{\infty}\left[\frac{Se_m(q,\eta_{\mathrm{s}})}{M_m^e(q)}\right]Se_m(q,\eta_{\mathrm{x}})Je_m(q,\xi_{\mathrm{s}})He_m(q,\xi_{\mathrm{x}})+\sum_{m=1}^{\infty}\left[\frac{So_m(q,\eta_{\mathrm{s}})}{M_m^o(q)}\right]So_m(q,\eta_{\mathrm{x}})Jo_m(q,\xi_{\mathrm{s}})Ho_m(q,\xi_{\mathrm{x}})\right),\ \xi_{\mathrm{x}}\ge\xi_{\mathrm{s}},\\ -2\pi i\left(\displaystyle\sum_{m=0}^{\infty}\left[\frac{Se_m(q,\eta_{\mathrm{s}})}{M_m^e(q)}\right]Se_m(q,\eta_{\mathrm{x}})Je_m(q,\xi_{\mathrm{x}})He_m(q,\xi_{\mathrm{s}})+\sum_{m=1}^{\infty}\left[\frac{So_m(q,\eta_{\mathrm{s}})}{M_m^o(q)}\right]So_m(q,\eta_{\mathrm{x}})Jo_m(q,\xi_{\mathrm{x}})Ho_m(q,\xi_{\mathrm{s}})\right),\ \xi_{\mathrm{x}}<\xi_{\mathrm{s}},\end{cases}\tag{28}$$

$$T(\mathbf{s},\mathbf{x})=\begin{cases}-2\pi i\dfrac{1}{J_{\mathrm{s}}}\left(\displaystyle\sum_{m=0}^{\infty}\left[\frac{Se_m(q,\eta_{\mathrm{s}})}{M_m^e(q)}\right]Se_m(q,\eta_{\mathrm{x}})Je_m'(q,\xi_{\mathrm{s}})He_m(q,\xi_{\mathrm{x}})+\sum_{m=1}^{\infty}\left[\frac{So_m(q,\eta_{\mathrm{s}})}{M_m^o(q)}\right]So_m(q,\eta_{\mathrm{x}})Jo_m'(q,\xi_{\mathrm{s}})Ho_m(q,\xi_{\mathrm{x}})\right),\ \xi_{\mathrm{x}}>\xi_{\mathrm{s}},\\ -2\pi i\dfrac{1}{J_{\mathrm{s}}}\left(\displaystyle\sum_{m=0}^{\infty}\left[\frac{Se_m(q,\eta_{\mathrm{s}})}{M_m^e(q)}\right]Se_m(q,\eta_{\mathrm{x}})Je_m(q,\xi_{\mathrm{x}})He_m'(q,\xi_{\mathrm{s}})+\sum_{m=1}^{\infty}\left[\frac{So_m(q,\eta_{\mathrm{s}})}{M_m^o(q)}\right]So_m(q,\eta_{\mathrm{x}})Jo_m(q,\xi_{\mathrm{x}})Ho_m'(q,\xi_{\mathrm{s}})\right),\ \xi_{\mathrm{x}}<\xi_{\mathrm{s}},\end{cases}\tag{29}$$

$$L(\mathbf{s},\mathbf{x})=\begin{cases}-2\pi i\dfrac{1}{J_{\mathrm{x}}}\left(\displaystyle\sum_{m=0}^{\infty}\left[\frac{Se_m(q,\eta_{\mathrm{s}})}{M_m^e(q)}\right]Se_m(q,\eta_{\mathrm{x}})Je_m(q,\xi_{\mathrm{s}})He_m'(q,\xi_{\mathrm{x}})+\sum_{m=1}^{\infty}\left[\frac{So_m(q,\eta_{\mathrm{s}})}{M_m^o(q)}\right]So_m(q,\eta_{\mathrm{x}})Jo_m(q,\xi_{\mathrm{s}})Ho_m'(q,\xi_{\mathrm{x}})\right),\ \xi_{\mathrm{x}}>\xi_{\mathrm{s}},\\ -2\pi i\dfrac{1}{J_{\mathrm{x}}}\left(\displaystyle\sum_{m=0}^{\infty}\left[\frac{Se_m(q,\eta_{\mathrm{s}})}{M_m^e(q)}\right]Se_m(q,\eta_{\mathrm{x}})Je_m'(q,\xi_{\mathrm{x}})He_m(q,\xi_{\mathrm{s}})+\sum_{m=1}^{\infty}\left[\frac{So_m(q,\eta_{\mathrm{s}})}{M_m^o(q)}\right]So_m(q,\eta_{\mathrm{x}})Jo_m'(q,\xi_{\mathrm{x}})Ho_m(q,\xi_{\mathrm{s}})\right),\ \xi_{\mathrm{x}}<\xi_{\mathrm{s}},\end{cases}\tag{30}$$

$$M(\mathbf{s},\mathbf{x})=\begin{cases}-2\pi i\dfrac{1}{J_{\mathrm{s}}J_{\mathrm{x}}}\left(\displaystyle\sum_{m=0}^{\infty}\left[\frac{Se_m(q,\eta_{\mathrm{s}})}{M_m^e(q)}\right]Se_m(q,\eta_{\mathrm{x}})Je_m'(q,\xi_{\mathrm{s}})He_m'(q,\xi_{\mathrm{x}})+\sum_{m=1}^{\infty}\left[\frac{So_m(q,\eta_{\mathrm{s}})}{M_m^o(q)}\right]So_m(q,\eta_{\mathrm{x}})Jo_m'(q,\xi_{\mathrm{s}})Ho_m'(q,\xi_{\mathrm{x}})\right),\ \xi_{\mathrm{x}}\ge\xi_{\mathrm{s}},\\ -2\pi i\dfrac{1}{J_{\mathrm{s}}J_{\mathrm{x}}}\left(\displaystyle\sum_{m=0}^{\infty}\left[\frac{Se_m(q,\eta_{\mathrm{s}})}{M_m^e(q)}\right]Se_m(q,\eta_{\mathrm{x}})Je_m'(q,\xi_{\mathrm{x}})He_m'(q,\xi_{\mathrm{s}})+\sum_{m=1}^{\infty}\left[\frac{So_m(q,\eta_{\mathrm{s}})}{M_m^o(q)}\right]So_m(q,\eta_{\mathrm{x}})Jo_m'(q,\xi_{\mathrm{x}})Ho_m'(q,\xi_{\mathrm{s}})\right),\ \xi_{\mathrm{x}}<\xi_{\mathrm{s}},\end{cases}\tag{31}$$

respectively, where $q=\left(\dfrac{ck}{2}\right)^2$, c is the half distance between two focuses of the elliptic coordinates, J_{s} and J_{x} are the Jacobian terms for the source point $\mathbf{s}$ and the field point $\mathbf{x}$, respectively, as shown below:

$$J_{\mathrm{s}}=c\sqrt{\left(\sinh(\xi_{\mathrm{s}})\cos(\eta_{\mathrm{s}})\right)^2+\left(\cosh(\xi_{\mathrm{s}})\sin(\eta_{\mathrm{s}})\right)^2},\tag{32}$$

$$J_{\mathrm{x}}=c\sqrt{\left(\sinh(\xi_{\mathrm{x}})\cos(\eta_{\mathrm{x}})\right)^2+\left(\cosh(\xi_{\mathrm{x}})\sin(\eta_{\mathrm{x}})\right)^2},\tag{33}$$

Se_m and So_m are the m^{th} order even and odd Mathieu functions (angular Mathieu functions) respectively, Je_m and Jo_m are the m^{th}order even and odd modified Mathieu functions (radial Mathieu functions) of the first kind, respectively, Ye_m and Yo_m are the m^{th} order even and odd the modified Mathieu functions of the second kind, respectively, He_m and Ho_m are the even and odd m^{th} order modified Mathieu functions (Mathieu-Hankel functions) of the third kind, respectively and are defined as

$$He_m = Je_m + iYe_m, \tag{34}$$

$$Ho_m = Jo_m + iYo_m, \tag{35}$$

M_m^e and M_m^o are the normalized constants and can be obtained by

$$M_m^e(q) = \int_{-\pi}^{\pi} \left(Se_m(q,\eta)\right)^2 d\eta = \pi, \tag{36}$$

$$M_m^o(q) = \int_{-\pi}^{\pi} \left(So_m(q,\eta)\right)^2 d\eta = \pi. \tag{37}$$

It is noted that U and M kernels in Eqs. (23), (26), (28) and (31) contain the equal sign of $\rho = \rho_{\mathbf{s}}$ and $\xi = \xi_{\mathbf{s}}$ while T and L kernels do not include the equal sign due to the discontinuity. For the unknown boundary densities, we apply the Fourier series and the eigenfunction expansion to approximate the boundary potential $u(\mathbf{s})$ and its normal derivative $t(\mathbf{s})$ along the circular and elliptic boundaries, respectively, as

$$u(\mathbf{s}) = \sum_{n=0}^{\infty} g_n \cos(n\phi_{\mathbf{s}}) + \sum_{n=1}^{\infty} h_n \sin(n\phi_{\mathbf{s}}), \ \mathbf{s} \in B, \tag{38}$$

$$t(\mathbf{s}) = \sum_{n=0}^{\infty} p_n \cos(n\phi_{\mathbf{s}}) + \sum_{n=1}^{\infty} q_n \sin(n\phi_{\mathbf{s}}), \mathbf{s} \in B, \tag{39}$$

and

$$u(\mathbf{s}) = \sum_{n=0}^{\infty} g_n Se_n(q,\eta_{\mathbf{s}}) + \sum_{n=1}^{\infty} h_n So_n(q,\eta_{\mathbf{s}}), \ \mathbf{s} \in B, \tag{40}$$

$$t(\mathbf{s}) = \frac{1}{J_{\mathbf{s}}}\left(\sum_{n=0}^{\infty} p_n Se_n(q,\eta_{\mathbf{s}}) + \sum_{n=1}^{\infty} q_n So_n(q,\eta_{\mathbf{s}})\right), \mathbf{s} \in B, \tag{41}$$

where g_n, h_n, p_n and q_n are the unknown coefficients of the boundary densities. The Jacobian term $J_{\mathbf{s}}$ may occur in the kernels of Eqs. (28)-(31), boundary densities of the Eq. (41) and elliptical boundary contour integration $(dB(\mathbf{s}) = J_{\mathbf{s}} d\eta_{\mathbf{s}})$. However, the Jacobian terms can be cancelled each other out and the orthogonal relations can be fully utilized in the elliptical boundary integration. The incident plane wave potential of Eq. (6) can be expressed in terms of the local polar and elliptic coordinates of the j^{th} cylinder, respectively, as shown below [Morse]:

$$u_I(\mathbf{x}_j) = \Lambda_j \sum_{n=0}^{\infty} \varepsilon_n (i)^n J_n(k\rho_{\mathbf{x}_j}) \cos(n(\phi_{\mathbf{x}_j} - \alpha)), \tag{42}$$

$$u_I(\mathbf{x}_j) = \Lambda_j \sqrt{8\pi} \left\{ \sum_{n=0}^{\infty} (i)^n \left[\frac{Se_n(q,\alpha)}{M_n^e(q)}\right] Se_n(q,\eta_{\mathbf{x}_j}) Je_n(q,\xi_{\mathbf{x}_j}) + \sum_{n=1}^{\infty} (i)^n \left[\frac{So_n(q,\alpha)}{M_n^o(q)}\right] So_n(q,\eta_{\mathbf{x}_j}) Jo_n(q,\xi_{\mathbf{x}_j}) \right\}, \tag{43}$$

where $\Lambda_j = e^{ik\left(X_j \cos(\alpha) + Y_j \sin(\alpha)\right)}$, X_j and Y_j are the Cartesian coordinates of the j^{th} cylinder's center by using the global observer.

2.5 Adaptive observer systems and linear algebraic equations

Since the boundary integral equations are frame indifferent, *i.e.* rule of objectivity is obeyed, an adaptive observer system is chosen to fully employ the property of degenerate kernels. Figure 1 shows the boundary contour integration for the circular and elliptical boundaries. It is worthy noted that the origin of the observer system can be adaptively located on the center of the corresponding circle or ellipse under integration to fully utilize the analytical properties of circular or elliptical boundaries, respectively. The dummy variable in the integration on the circular and elliptical boundaries are only the angle $\phi_{\mathbf{s}}$ and $\eta_{\mathbf{s}}$ instead of the radial coordinates $\rho_{\mathbf{s}}$ and $\xi_{\mathbf{s}}$, respectively. By using the adaptive observer system, all the boundary integrals can be determined analytically free of principal value. In order to calculate the unknown coefficients, collocation of boundary nodes on circular and elliptical boundaries to match boundary conditions are needed. Therefore, we obtain the linear algebraic equations from Eqs. (20) and (21) as shown below [10]:

$$[U]\{t\}=[T]\{u\}, \tag{44}$$

$$[L]\{t\}=[M]\{u\}. \tag{45}$$

All the unknown coefficients can be obtained easily by using the linear algebraic equation of Eqs. (44) and (45). Then, the unknown boundary data can be determined and the interior potential is obtained by substituting the boundary data into Eq. (18).

3. Illustrative examples

Case 1 A single elliptical cylinder

The first case is a single elliptical cylinder. The half lengths of major and minor axes are $a_1=10$ and $b_1=1.5$, respectively and the water depth is $h=10$. The analytical solution was found by Goda and Yoshimi [2]. Au and Brebbia [3] used the BEM to revisit this problem and their results are consistent with ours. Regarding this problem, we can also obtain the analytical solution for the radiative field by using the present approach as shown below:

$$\begin{aligned} u_R(\mathbf{x}) = -4\sqrt{\frac{2}{\pi}}\Bigg\{ &\sum_{n=0}^{\infty}(i)^n\left[\frac{Se_n(q,\alpha)}{M_n^e(q)}\right]Se_n(q,\eta_{\mathbf{x}})\frac{Je_n'(q,\xi_1)}{He_n'(q,\xi_1)}He_n(q,\xi_{\mathbf{x}}) \\ &+\sum_{n=1}^{\infty}(i)^n\left[\frac{So_n(q,\alpha)}{M_n^o(q)}\right]So_n(q,\eta_{\mathbf{x}})\frac{Jo_n'(q,\xi_1)}{Ho_n'(q,\xi_1)}Ho_n(q,\xi_{\mathbf{x}})\Bigg\}, \end{aligned} \tag{46}$$

where $\xi_1=\tanh^{-1}(b_1/a_1)$ denotes the elliptical boundary using the elliptical coordinates. Figures 2 shows the resultant force of the total potential from two different incident angles ($\alpha=30^\circ$ and 60°). After comparing with the Au and Brebbia's data [3], our results are acceptable.

Case 2 Two parallel identical elliptical cylinders

In the second case, we revisit the problem of two parallel identical elliptical cylinders subject to the incident plane wave as shown in Fig. 3(a) which has been considered by Chatjigeorgiou and Mavrakos [6]. The half lengths of major and minor axes are $a_1=a_2=1$ and $b_1=b_2=0.25$, respectively. The distance between the centers of two cylinders is $d=2$ and the water depth is $h=1.5$. Figure 4 shows the wave force for the incident angle of $\alpha=60^\circ$ and the normalized parameter is $\rho_w g(A/2)a_1^2$ where ρ_w denotes the density of water. To see the validity of present approach, we also used the conventional BEM to verify the present results. Agreement is made.

Case 3 One circular and one elliptical cylinder

Based on the adaptive observer system, the present approach is employed to solve the water wave problem containing one circular and one elliptical cylinder at the same time as shown in Fig. 3(b). The radius of the circular cylinder is $a_2=0.5$ and the other geometry data and normalized parameter are the same with the case 1. The resultant forces for incident angles ($\alpha=90^\circ$ and -90°) are shown in Figs. 5. The present results are consistent with the data of the conventional BEM.

.

4. Conclusions

In this paper, we have successfully extended the null-field BIEM to solve the water wave scattering problems containing multiple circular and elliptical cylinders together. By employing the adaptive observer system and the degenerate kernels for the fundamental solution in terms of the polar and elliptic coordinates, the water wave scattering problems containing circular and elliptical cylinders at the same time were solved in a semi-analytical way. This method also belongs to a meshless method since collocation points on the boundaries are only required.

References

[1] MacCamy R. C. and Fuchs R. A. "Wave force on piles: A diffraction theory", Technical Memorandum No. 69, *U. S. Army Coastal Engineering Research Center (formerly Beach Erosion Board)*, 1954.

[2] Goda Y. and Yoshimura T., "Wave force on vessel tired at offshore dolphins", *Proceedings 13th Coastal Engineering Conference*, Vancouver, B. C., Canada, Chap. 96, Vol. III, (1972), pp 1723-1742.

[3] Au M. C. and Brebbia C. A., "Diffraction of water waves for vertical cylinders using boundary elements", *Applied Mathematical Modelling*, Vol. 7, (1983), pp 106-114.

[4] Spring B. H. and Monkmeyer P. L. "Interaction of plane waves with vertical cylinders", *Proceedings 14th Coastal Engineering Conference*, Copenhagen, Denmark, Vol. III, (1974), pp 1828-1845.

[5] Linton C. M. and Evans D. V. "The interaction of waves with arrays of vertical circular cylinders", *Journal of Fluid Mechanics*, Vol. 215, (1990), pp 549-569.

[6] Chatjigeorgiou I. K. and Mavrakos S. A., "Hydrodynamic diffraction by multiple elliptical cylinders", *24th International Workshop on Water Waves and Floating Bodies*, Zelenogorsk, Russia, (2009).

[7] Særmark KA (1959) A note on addition theorems for Mathieu functions. ZAMP 10: 426-428.

[8] Chen J. T., Kao S. K., Lee W. M. and Lee Y. T., "Eigenproblems of a multiply-connected domain with circular boundaries using the multipole Trefftz method", *Engineering Analysis with Boundary Elements*, (2009), Accepted.

[9] Lee W. M. and Chen J. T., "Free vibration analysis of a circular plate with multiple circular holes by using multipole Trefftz method", *Computer Modeling in Engineering Science*, (2009), Accepted.

[10] Chen J. T., Lee Y. T. and Lin Y. J., "Interaction of water waves with arbitrary vertical cylinders using null-field integral equations", *Applied Ocean Research*, Vol. 31, (2009), pp 101-110.

[11] Morse P. and Feshbach H., "*Method of Theoretical Physics*", McGraw-Hill, New York, (1953).

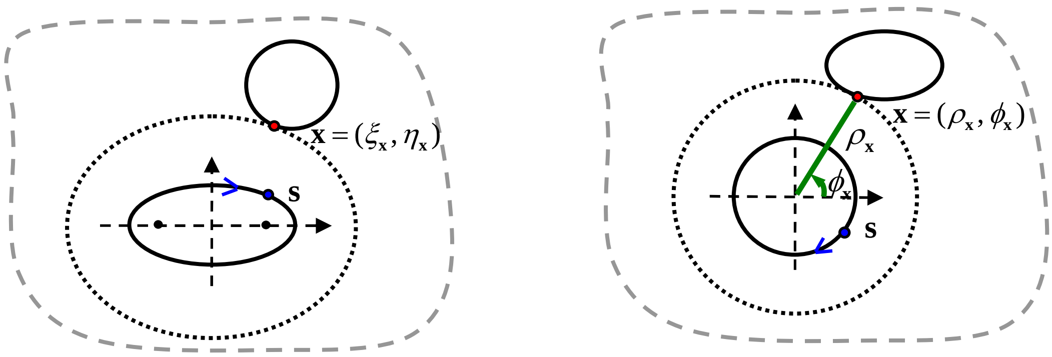

(a) Observer at the center of the elliptical boundary under integration using the elliptic coordinates.

(b) Observer at the center of the circular boundary under integration using the polar coordinates.

Figs. 1 An adaptive observer system.

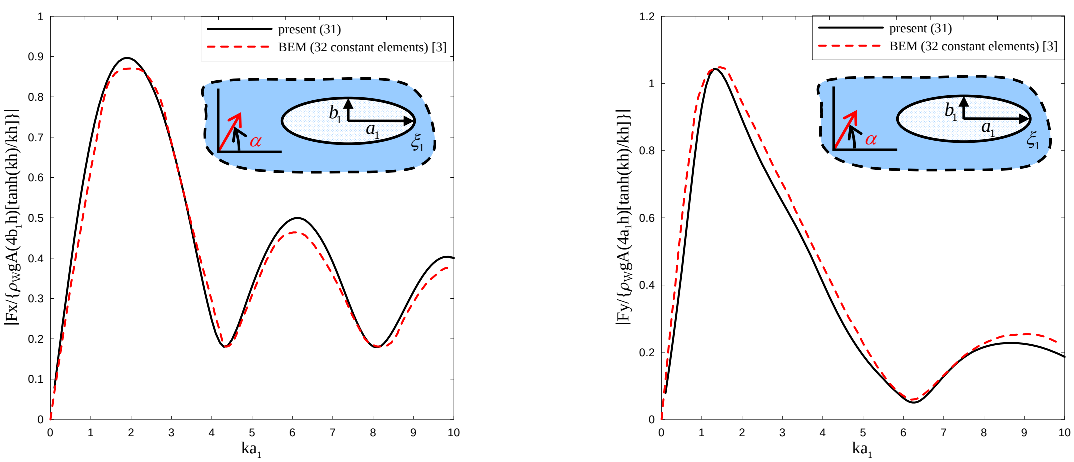

(a) F_x, $\alpha = 30^\circ$

(b) F_y, $\alpha = 60^\circ$

Figs. 2 Resultant forces of an elliptical cylinder.

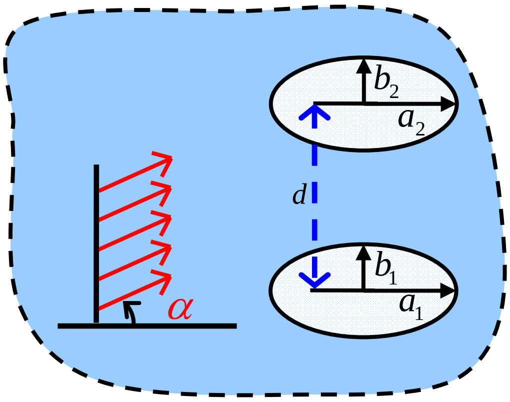

(a) Two parallel identical elliptical cylinders,

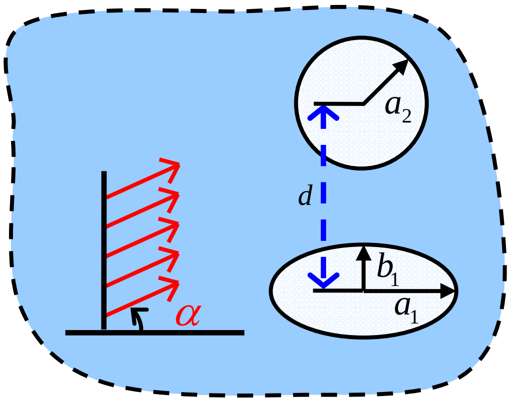

(b) One circular and one elliptical cylinder.

Figs. 3 Sketch of the problems

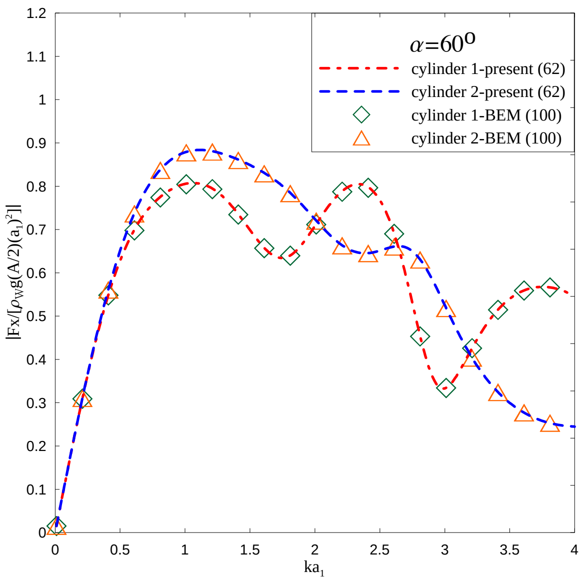

(a) F_x, $\alpha = 60^{\circ}$.

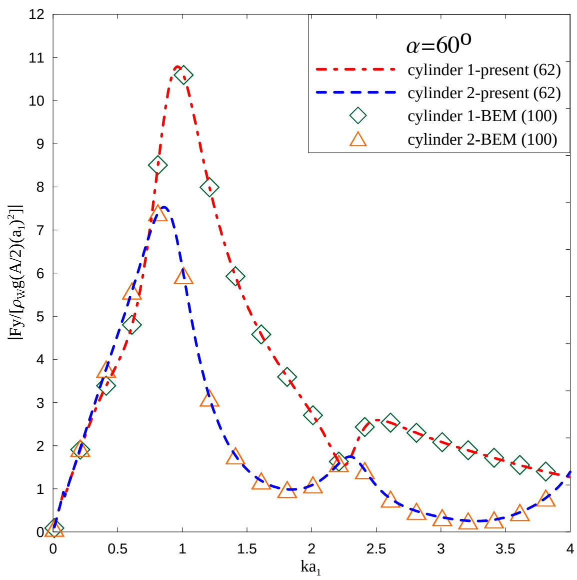

(b) F_y, $\alpha = 60^{\circ}$.

Figs. 4 Resultant forces of two parallel identical elliptical cylinders.

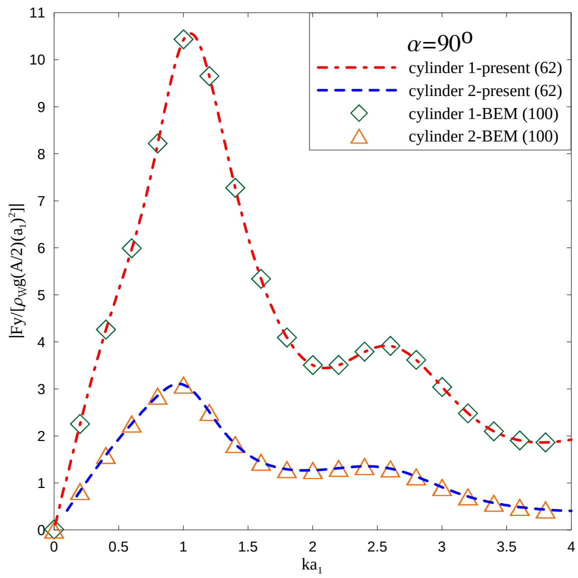

(a) F_y, $\alpha = 90^{\circ}$.

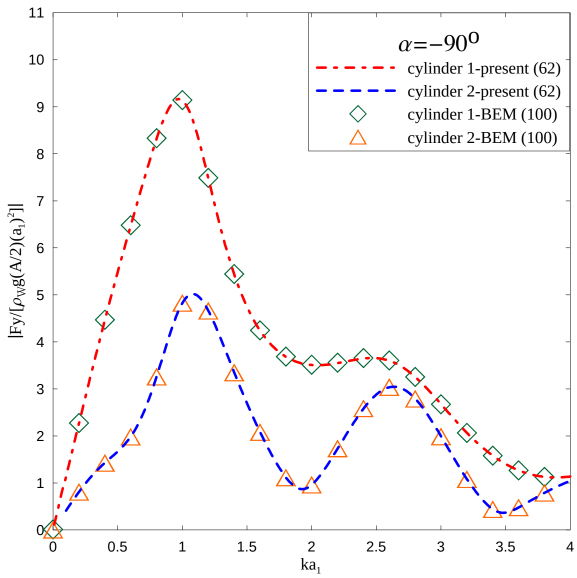

(b) F_y, $\alpha = -90^{\circ}$.

Figs. 5 Resultant forces of two cylinders containing one circular and one elliptical cylinder.